ADVANCED FUNCTIONAL MATERIALS
www.afm-journal.de

Polymorphism in Crystalline Microfibers of Achiral Octithiophene: The Effect on Charge Transport, Supramolecular Chirality and Optical Properties

Francesca Di Maria, Eduardo Fabiano, Denis Gentili, Mariano Biasiucci, Tommaso Salzillo, Giacomo Bergamini, Massimo Gazzano, Alberto Zanelli, Aldo Brillante, Massimiliano Cavallini, Fabio Della Sala, Giuseppe Gigli, and Giovanna Barbarella**

Polymorphic crystalline microfibers from an achiral octithiophene with one S-hexyl substituent per ring are separately and reproducibly grown with the same characteristics on various solid surfaces, including the interdigitated electrodes/SiO_2 surface of a bottomcontact field-effect transistor. The arrangement of the same molecule in two diverse supramolecular structures leads to markedly different electronic, optical, and charge mobility properties. The microfibers—straight and yellow emitting or helical and red emitting—exhibit *p*-type charge transport characteristics, with the yellow ones showing a charge mobility and on/off current ratio of one and three orders of magnitude, respectively, greater than the red ones. Both forms show circular dichroism signals with significant differences from one form to the other. DFT calculations show that the octithiophene exists in two different quasi-equienergetic conformations aggregating with diverse orientations of the substituents. This result suggests that the observed polymorphism is conformational in nature. The self-assembly, driven by sulfur–sulfur non-bonding interactions, amplifies the small property differences between conformers, leading to quite different bulk properties.

1. Introduction

Polymorphism in organic crystals, namely the existence of different crystalline forms for the same substance, is a phenomenon of considerable fundamental and technological relevance.[1] The intermolecular interactions and the mechanisms leading to different crystal arrangements are matter of intense studies aimed to achieve the control and prediction of solid-state structures.[2] Polymorphism has acquired great importance for organic solids of pharmaceutical interest, since the solid-state packing may affect biological activity or other features such as rate of dissolution or shelf life.[3] In conjugated materials, which are of major importance in nanotechnologies, solid-state molecular packing plays a crucial role in controlling the

Dr. F. Di Maria, Dr. M. Gazzano, Dr. A. Zanelli, Dr. G. Barbarella
ISOF, MIST.E-R, Mediteknology
Consiglio Nazionale Ricerche
Via P. Gobetti 101, I-40129, Bologna, Italy
E-mail: francesca.dimaria@isof.cnr.it; giovanna.barbarella@isof.cnr.it
Dr. E. Fabiano, Dr. F. Della Sala
NNL CNR-Istituto Nanoscienze
Via Arnesano, I-73100, Lecce, Italy
Dr. D. Gentili, Dr. M. Cavallini
ISMN, Consiglio Nazionale Ricerche
Via P. Gobetti 101, I-40129, Bologna, Italy
Dr. M. Biasiucci
NNL-CNR Nanoscience Institute
c/o Dpt, Fisica Ed. G. Marconi
Center for Life, NanoScience
La Sapienza University and IIT
Viale Regina Elena 295, I-00161, Roma, Italy
T. Salzillo, Prof. A. Brillante
Dpt of Industrial Chemistry Toso Montanari
University of Bologna
Viale Risorgimento 4, I-40136, Bologna, Italy
Dr. G. Bergamini
Dpt of Chemistry Giacomo Ciamician
University of Bologna
Via Selmi 2, I-40126, Bologna, Italy
Prof. G. Gigli
Dpt Ingegneria Innovazione
Università del Salento
Via Arnesano, I-73100, Lecce, Italy

DOI: 10.1002/adfm.201400534

ADVANCED FUNCTIONAL MATERIALS
www.afm-journal.de

functional properties. Cases of polymer-induced[4] or solvent-[5] and substrate-induced[6] polymorphism observed in pentacene and its derivatives have been described and related to charge transport properties. The relationship between polymorphism and functional properties in other families of π-conjugated oligomers[7,8] and polymers, including poly(3-hexyl-thiophene)[9–11] has also been explored.

A few cases of polymorphism in thiophene oligomers have been reported, most of them concerning conformational polymorphism in single crystals,[12,13] where different conformations of the same molecule pack in different ways. Conformational poly-morphism generally occurs with molecules with flexible torsions.[1] A thiophene derivative, ROY, namely 5-methyl-2-[(2-nitrophenyl) amino]-3-thiophenecarbonitrile, an intermediate in the production of the pharmaceutical olanzapine, has seven stable and a few unstable, structurally characterized, conformational polymorphs.[14,15] The name ROY derives from the color of its red, orange, and yellow polymorphs and the polymorphism is due to variations in the C–N–C–S torsion angle. Early studies on unsubstituted quater- and sexithiophene have shown that these compounds form different polymorphs having either a completely flat or a slightly tilted conformation with trans-trans configuration of adjacent rings and different packing arrangements.[16–19] Orange and yellow single crystals of a head-to-head S–CH_3 substituted quaterthiophene[20,21] and a tetramethyl substituted sexithiophene with the same regiochemistry of substitution,[22] were separated at room temperature and displayed different conformations and crystal packings. In other cases the conformational polymorphism was induced by alkyl side chains which were either nearly perpendicular or parallel to the molecular backbone[23] or by a trans-trans or cis-trans configuration of the thiophene rings.[24]

We report here the first case of polymorphism in octithiophene crystalline microfibers spontaneously self-assembled on solid substrates. The octithiophene in question is a "sulfur overrich" oligomer with one S-hexyl substituent per ring and head-to-head regiochemistry of substitution.[25] The octamer was designed as part of a chemical strategy aimed to obtain oligothiophenes with an intrinsic tendency to self-assemble anisotropically in nano and microfibers by virtue of intra- and inter-molecular sulfur-sulfur non-bonding interactions controllable via organic synthesis with different building blocks.[25] It formed thermodynamically very stable, red emitting, crystalline microfibers displaying the same helical morphology independently of the type of surface on which they were grown. We have now been able to obtain polymorphic crystalline microfibers of the octithiophene, stable, straight and yellow emitting, which can be separately grown on solid substrates and characterized. We demonstrate that the yellow microfibers display significantly different electronic, optical and charge transport properties from the red emitting ones. Theoretical calculations on conformational energies and aggregation tendencies of the octithiophene, together with X-ray diffraction data, indicate that the polymorphism observed for the microfibers is the result of the interplay of slightly different conformations and different packing organizations.

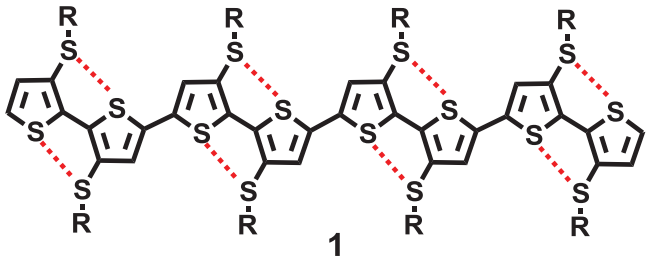

Figure 1. Molecular structure of octithiophene **1** (R = C_6H_{13}). Dotted red lines highlight intramolecular S···S interactions according to DFT calculations (S···S distance = 3.07–3.09 Å).

2. Results and Discussion

The molecular structure of the microfibers forming octithiophene, namely 3,3′,3‴,3⁗,3⁗′,4″,4⁗,4⁗′-octakis(hexylsulphanyl)-octithiophene (**1**), is reported in **Figure 1**.

Octithiophene **1**, with one S-hexyl chain per ring and head-to-head substitution pattern was synthesized through a sequence of selective monobrominations and Suzuki coupling steps, as already described.[25] When **1** was synthesized for the first time it was separated as a dark-red, red-emitting, microcrystalline powder. We have now been able to obtain the same compound in the form of a yellow, yellow-emitting, microcrystalline powder (**Figure 2**). In $CDCl_3$ the yellow and red powders display the same mass spectrum and the same proton and carbon-13 spectra, corresponding to those already described.

However, they show different differential scanning calorimetry (DSC) plots: a peak at 73.0 °C (onset 63.3 °C) and a ΔH value of 24.5 J/g for the red powder and a peak at 70.7 °C (onset 64.2 °C) and a ΔH value of 31.4 J/g for the yellow one, indicating that the latter is slightly more stable than the former (Figure 4S, Figure 5S). No signs of interconversion of one form to the other were observed. The yellow and red powders showed different X-ray diffraction profiles (Figure 2).

A very intense small angle reflection was present in both profiles (yellow d = 1.96 nm; red d = 1.74 nm). The profile of

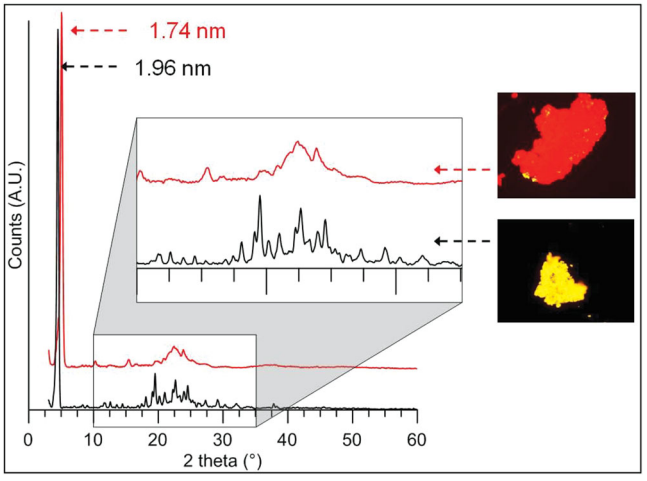

Figure 2. Plots of X-ray analysis of the microcrystalline powders of octamer **1**. The insets are microscopy fluorescence images of the red and yellow forms.

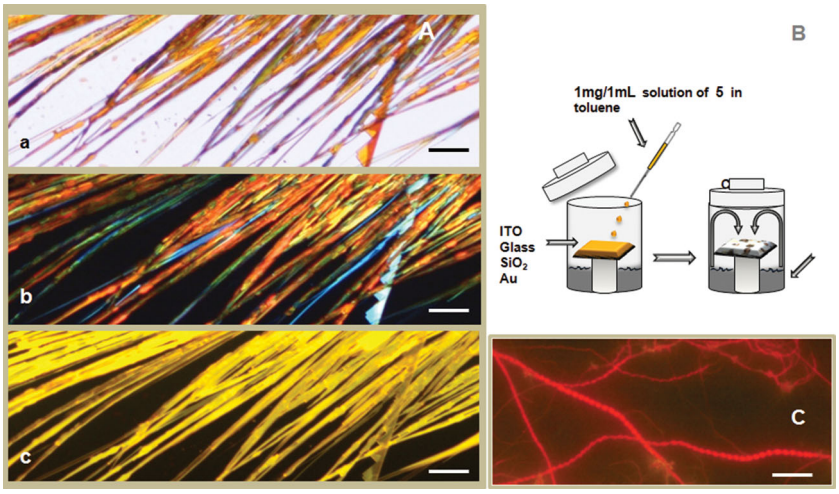

Figure 3. A) Light transmission microscopy image (a), microscopy image with cross polarizers oriented parallel and perpendicular to the images axes (b) and fluorescence microscopy image (c) of the yellow microfibers grown on glass from the yellow powder. Bars: 50 μm. B) Sketch illustrating the preparation of the microfibers. C) Fluorescence microscopy image of helical red microfibers obtained from the red powder (see also reference [25]). Bar: 50 μm.

the yellow form showed sharper and more resolved reflections indicating that the crystalline domains are of better quality than those of the red form, which shows broadened and overlapped reflections.

The identification of the yellow powder was the result of an empirical search (for more details see Supporting Information.) Currently, we are pursuing efforts to acquire full control on the formation of the yellow or red powders from solutions of **1**. However, having in hand both forms, we can control the formation of one or the other simply by seeding with a previous crystal of the desired form.

Microfibers from the yellow or red powder (**Figure 3**A,C) were separately prepared starting from 1 mg/1 mL solution (6.3×10^{-4} M) of the powder in toluene, a solvent in which **1** is very soluble. Drops of the solution were put on a solid support (glass or ITO or SiO_2 of a field-effect transistor device with gold contacts) located inside a glass cylinder containing at the bottom CH_3CN, a solvent in which **1** is insoluble (Figure 3B).

The drops of octamer in toluene diffuse on the substrate and when the CH_3CN vapours come in touch with the toluene solution crystallization in the form of microfibers takes place. Afterwards the substrate is removed and allowed to dry on a Petri dish. The process takes place at ambient T. The formation of the microfibers (Figure 3 and Figure 6S, Figure 7S, Figure 8S) is highly reproducible provided the concentration of the starting solution in toluene is kept between 10^{-3} and 10^{-4} M. It is known that nucleation to form specific polymorfs is often driven by self-association in solution.[1,26] On this basis our hypothesis is that at the concentration employed octithiophene **1** is still partially aggregated as it was in the powder and the aggregates act as crystallization nuclei for the formation of the microfibers. This hypothesis is in agreement with the fact that: 1) X-ray diffraction data (see below) indicate that the crystal phase of the microfibers is the same as that of the respective powders, 2) when a mixture of yellow and red powders is employed (at the same concentration in toluene), mixed yellow and red microfibers are obtained (Figure 11S). The yellow and red microfibers shown in Figure 3 are very stable and always display the same morphology independently of the type of solid support employed. Figure 3A shows the light transmitted microscopy image with parallel (a) and crossed (b) polarizers and the fluoresce microscopy image (c) of the microfibers obtained on glass from the yellow powder. When using crossed polarizers they exhibit birefringence and by rotating progressively the polarized light by 360° exstinguish in four positions, indicating that they are crystalline. No matter what the substrate employed is, the yellow microfibers invariably display a high aspect ratio being tens of micrometers long and a few micrometers wide, while their thickness is submicrometric (Figure 10S).

For a satisfying identification and characterization of polymorphs a combination of various techniques is required.[1] Hence, a comprehensive description of the yellow microfibers is reported below in parallel with that of the red microfibers, for comparison.

2.1. Structural Characterizations

Figure 4 compares the X-ray diffraction plots and the Raman spectrum in the 600–2000 cm^{-1} region of the yellow and red microfibers separately grown on glass from the corresponding powders. Concerning the X-ray plots, the yellow microfibers show several sharp intense reflections attributable to further orders (up to the seventh) of the 1.96 nm periodicity, while the red microfibers only show two main peaks (d = 1.74, 1.54 nm). The full width at half-maximum (FWHM) of the most intense peaks of the yellow and red microfibers are FWHM = 0.079° and 0.173°, respectively. The length of the crystal domains, estimated with Scherrer method, are L = 102 nm and L = 46 nm, respectively.

Furthermore, both types of microfibers show a high crystal orientation, in particular in the yellow phase as demonstrated by the high order of repetition of the main reflection. Peak widths indicate that the length of the coherent domains of the yellow polymorph is twice that of the red one.

Concerning the Raman spectra reported in Figure 4B, it is seen that both the yellow (yellow plot) and red (red plot) microfibers display exactly the same pattern. The 600–2000 cm^{-1} spectral region shows the vibrations typical of oligothiophenes.[27] In particular, near 1450 cm^{-1} the C=C and C–C stretching are present, while near 1200 cm^{-1} there is the signal of the inter-ring C–C vibrations and near 730 cm^{-1} the signal corresponding to the vibration of ring C–S–C deformation. Thus, the Raman spectra show that the yellow and red microfibers are made of the same molecular material. Unfortunately, the signals in the 0–200 cm^{-1} region, related to the crystalline network, are too weak to allow any sound description of the differences between the two polymorphs (Figure 9S).

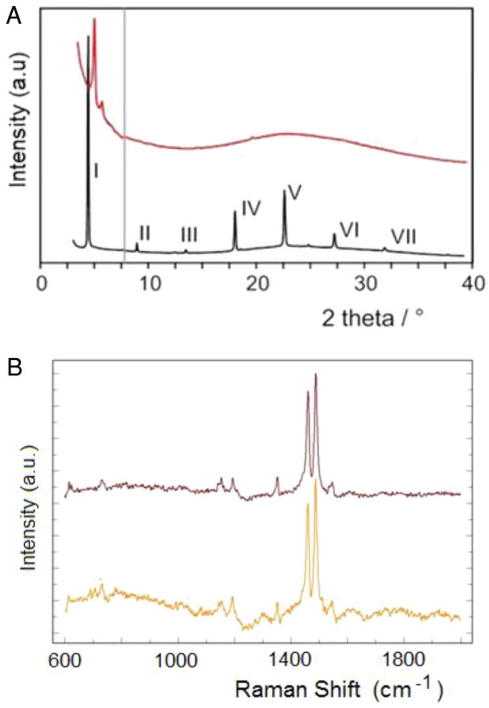

Figure 4. A) (a) X-ray diffraction pattern of yellow (black trace) and red (red trace) microfibers grown on glass. The romans highlight the consecutive orders of the 1.96 nm periodicity. B) Raman spectrum in the 600–2000 cm^{-1} region of the yellow (yellow trace) and red (red trace) microfibers on glass.

2.2. Optical Characterizations

Figure 5A displays the laser scanning confocal microscopy (LSCM) image and the spatially resolved spectra of the yellow microfibers grown on ITO. The LSCM image and spatially resolved spectra of a sample with yellow and red microfibers grown on ITO from mixed yellow and red powders are reported in Figure 11S, showing that the emission wavelength of the red microfibers is red-shifted by about 70 nm, indicating that the different assembly and the different intermolecular interactions result in a lower energy excited state formation. Figure 5B displays the emission spectra and fluorescence anisotropy of yellow and red microfibers separately grown on glass and obtained using a conventional spectrofluorimeter by positioning the sample holder with an angle of 30° to the excitation beam. Another tool to investigate the assembly and the structure of the fibers is fluorescence anisotropy, a dimensionless quantity defined as: $r = (I_{\parallel} - I_{\perp}) / (I_{\parallel} + 2I_{\perp})$, where $I_{\parallel}$ and $I_{\perp}$ are the emission intensities registered when the emission and excitation polarizers are oriented parallel and perpendicular, respectively.[28,29] For a simple fluorophore in a rigid matrix, depolarization can occurr because of the electronic properties of the excited states involved in absorption and emission.[30–32] In a fluid solution, depolarization takes place by rotation of the molecule during the excited-state lifetime. In an array of differently oriented, closely packed fluorophores, depolarization can occur by energy migration from the absorbing to the emitting species. When the molecule is blocked, in the solid state or at very low temperature, the depolarization can only occur by energy migration among the chromophores. The anisotropy value for the yellow microfibers sample was found to be 0.11 while was practically 0 for the red microfibers even though the chromophores are close packed in both cases. These

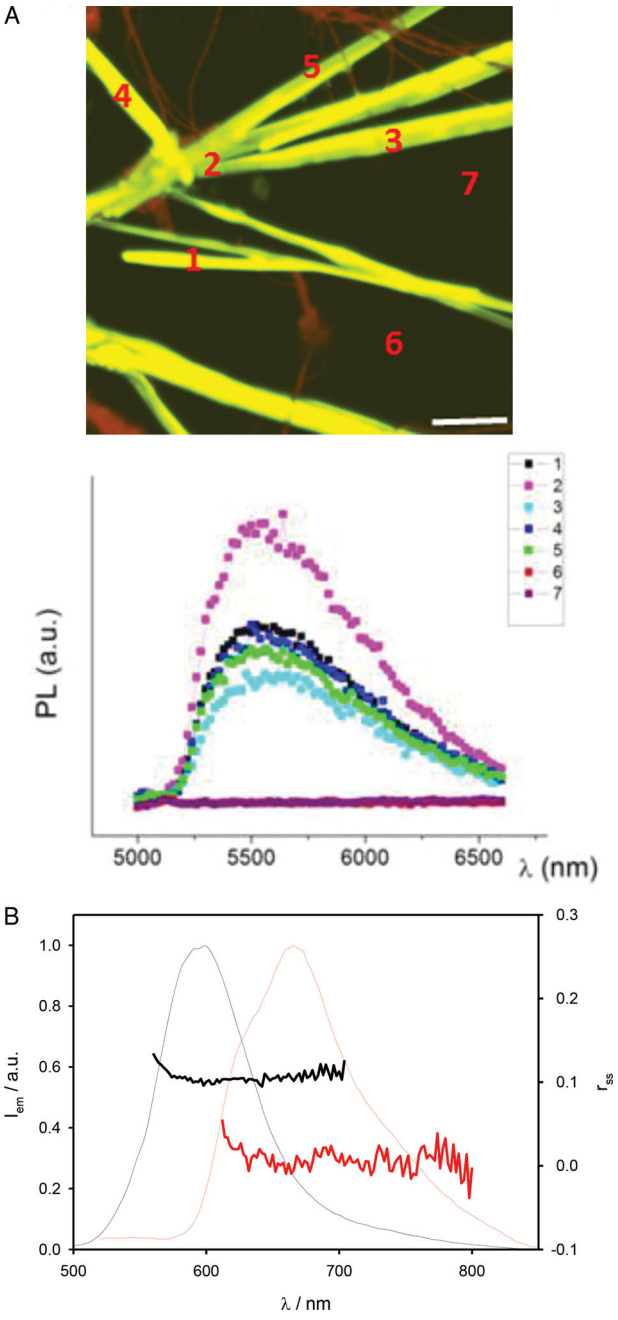

Figure 5. A) Laser scanning confocal microscopy image and spatially resolved photoluminescence spectra of the yellow microfibers grown on ITO. Bar: 20 μm. B) Normalised fluorescence spectra and steady state anisotropy of yellow (black line) and red microfibers (red line) grown on glass (λ_{ex} = 480 nm). Note that in Figure 5A each one of the spectra is relative to a single fiber while the spectrum of Figure 5B is relative to the envelope of fibers included into the surface of the irradiation spot (4×9 mm^2).

results demonstrate that in the yellow microfibers the transition dipole moments are oriented nearly parallel and modest light depolarization takes place during the lifetime. In the case of the red microfibers, the fluorescence anisotropy reaches the steady-state value of r = 0 within its lifetime, thus indicating that the information on molecular orientation is completely lost after a few energy-transfer steps. This observation is in agreement with the optical and atomic force microscopy, with the morphology, in which a helical arrangement is demonstrated for the red microfibers, and with the theoretical calculations reported below.

To complete the optical characterizations, circular dichroism (CD) spectra were run for the yellow and red microfibers separately grown on glass. For each type of microfibers the spectra of two different samples (reversed in sign) are reported in **Figure 6**. The CD spectra of the red microfibers are the same as those already reported by us and interpreted as being due to the interplay of molecular and supramolecular helicity.[25] Since octamer **1** lacks asymmetrically substituted carbon atoms, no CD signal is observed in solution. The optical activity observed in the solid state is the effect of hindered rotations about the thienyl-thienyl inter-ring bonds caused by the freezing of the molecule on the solid support.[33] Hindered rotations about a thienyl-thienyl linkage have the potentiality to generate enantiomers, as in the case of tetra-*ortho* substituted biphenyls in which the freezing of the interring C–C rotation generates stereoisomers displaying axial chirality.[34] The phenomenon is named *atropisomerism* and has profound implications in drugs synthesis.[35,36] When **1**, which has seven inter-ring bonds, is deposited on a solid support, scalemic (enantiomerically enriched) mixtures are formed, which are made of different conformers in the yellow and red polymorphs. As soon as the first molecule of **1** is locked on the surface of the sustrate, it looses all symmetry elements and becomes chiral.[33] The handedness of the first molecule then induces preferential handedness of the same sign on the following ones, causing chirality amplification. Since the one or the other handedness sign of the first molecule have equal probabilities, different samples may display opposite chiralities, as is indeed shown in Figure 6. In the red microfibers the weak intermolecular interactions due to the helical morphology induce an additional supramolecular component to the overall chirality of the system. Figure 6B shows that the CD spectra of the red microfibers present extensively enlarged bands with respect to those of the yellow polymorph, which are precisely the signature of supramolecular helicity.[37–39] It is worth noting that, as far as we know, the yellow microfibers are the first example reported so far of microfibers with straight morphology displaying a CD spectrum. Apparently, a helical morphological habit only adds a supramolecular component to the chirality but it is not a necessary condition to observe a CD spectrum. This finding is important since the non linear optical properties related to the chirality of supramolecular assemblies may open the door to a new generation of functional materials.[40]

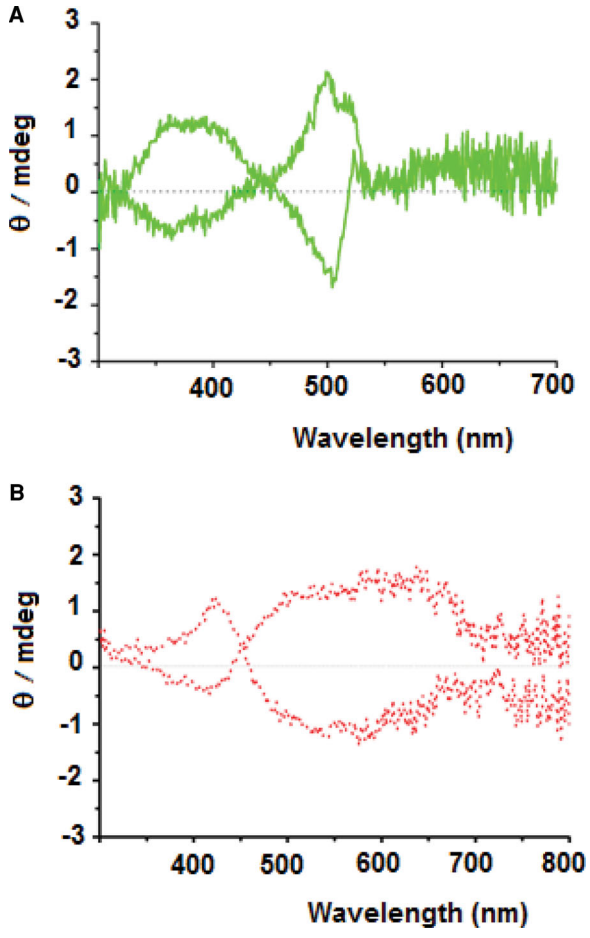

Figure 6. Circular dichroism spectra of two different samples of the yellow (A) and red (B) microfibers grown on glass.

2.3. Electrical Characterization

The semiconducting properties of the yellow and red microfibers were measured using them as active layers in organic field-effect transistors (OFETs) built in bottom-gate, bottom-contact architecture.[41] The microfibers were directly grown on interdigitated gold source and drain microelectrodes prefabricated on the octadecyltrichlorosilane (OTS) self-assembled monolayer (SAM)-treated Si/SiO_2 substrate (SI for details). Saturated charge mobilities were measured in vacuum (10^{-5} mbar) with a drain voltage $V_D = -60$ V and calculated by estimating the coverage of the device on the basis of optical microscopy images. In addition, to ensure full consistency between the devices based on different microfibers, bias range and voltage steps were kept constant. **Figure 7**A and B show the optical images of the OFET devices with separately grown yellow and red microfibers (a), the output features (b), the AFM images (c) with details (d) and the corresponding AFM profiles (e). The electrical transfers in saturation regime are displayed in Figure 12S. It is seen that the AFM images show the peculiar features of yellow and red microfibers, namely straight morphology for the former and helical morphology for the latter, with comparable submicrometric thickness. Both types of microfibers exhibit *p*-channel field-effect characteristics. However, the OFET based on yellow microfibers clearly shows a better field-effect performance than

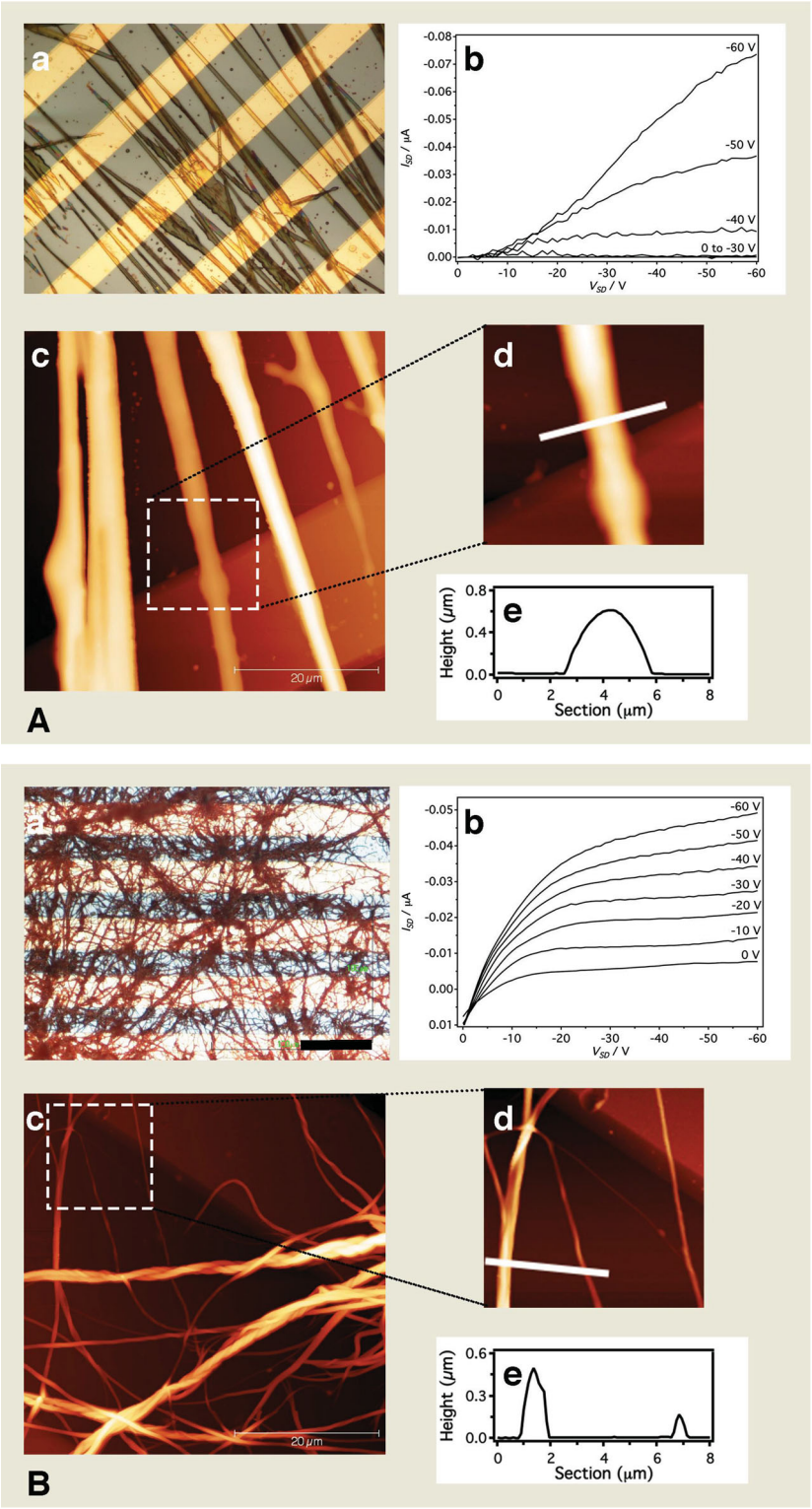

Figure 7. (A) Optical micrographs (a) (scale bar: 50 μm), output plots at various gate voltages (b), AFM topography (c,d) and AFM profile (e) of yellow microfibers grown directly on the interdigitated electrodes/SiO_2 surface of a bottom-contact field-effect transistor. (B) Optical micrographs (a) (scale bar: 50 μm), output plots at various gate voltages (b), AFM topography (c,d) and AFM profile (e) of red microfibers grown directly on the interdigitated electrodes/SiO_2 surface of a bottom-contact field-effect transistor.

that based on red microfibers. Saturated hole mobility, μ_{sat}, and I_{ON}/I_{OFF} ratio are indeed one and three orders of magnitude higher, respectively, than those obtained with the red microfibers. In particular, μ_{sat}, threshold voltage (V_T), and I_{ON}/I_{OFF} are determined to be 2.20×10^{-4} cm^2 V^{-1} s^{-1} (maximum value = 6.83×10^{-4} cm^2 V^{-1} s^{-1}), –25 V, and 10^4 for the yellow microfibers and 2.05×10^{-5} cm^2 V^{-1} s^{-1} (maximum value = 2.64×10^{-5}), –22 V, and 10^1 for the red ones. The modest charge mobilities reported could certainly be increased by optimization of the OFET devices or manipulation of the organization of the microfibers on the surface. For example, we have already demonstrated that controlling the self-assembly of microfibers forming thiophene oligomers by confinement effects provides an increase in charge mobility up to three orders of magnitude.[42] However, to this stage our objective was only to demonstrate that the microfibers were electroactive and displayed very different characteristics. Considering that the yellow and red microfibers are polymorphic structures, the results indicate that the different electrical properties are strongly related to the molecular packing, which in the case of the yellow polymorph favors significantly the charge transport. This result is in agreement with the X-ray diffraction data reported above, showing that the interlayer distance in the red phase is greater than in the yellow one. The yellow phase, both in powder or microfibers, has a higher tendency to form more ordered crystalline domains, allowing better orbitals overlap and more efficient electron transfer.

2.4. Electrochemical Characterization

A comparison of the cyclic voltammograms of yellow and red microfibers separately grown on ITO electrodes is reported in **Figure 8**. The current was normalized to compensate the differences in coating masses. The oxidation onset potential of the yellow microfibers was E_{ox}(onset) = 0.70 V vs. SCE (0.20 V vs. Fc/Fc^+) and the reduction onset potential was E_{red}(onset) = –1.50 V vs. SCE (–1.70 V vs. Fc/Fc^+). In agreement with the UV-vis blue-shift, the electrochemical band gap of the yellow microfibers was 2.20 eV, that is 0.08 eV (99 nm) smaller than that of the red microfibers, mainly because of the decrease in the HOMO energy (–5.30 eV).

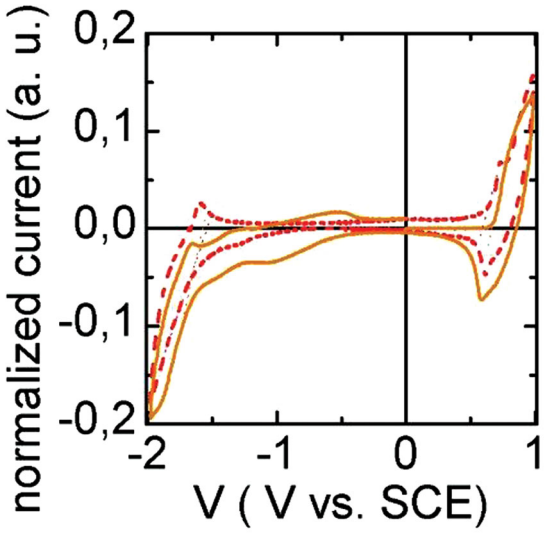

Figure 8. Voltammograms of yellow and red microfibers in PC-0.1 M $TEABF_4$ (yellow and dotted red line, respectively). The microfibers were separately grown on the ITO substrate.

2.5. Theoretical Calculations

Owing to the heavy computational requirements due to the large number of sulfur atoms, no high level theoretical calculations have been carried out so far on sulfur overrich octamers. To elucidate the capability of octamer **1** to self-aggregate in different forms, we have now calculated the conformational preferences and aggregation modalities for the octamer substituted with $S\text{-}CH_3$ instead of $S\text{-}C_6H_{13}$ groups. The calculations have been performed at the density functional theory level using the BLOC-D3 eta-GGA functional[43] (which includes semiempirical D3 dispersion corrections). A preliminary screening of possible equilibrium geometries was carried out using the def2-SV(P) basis set. Final calculations were performed using a def2-TZVPP basis set. The consistency of the obtained results was evaluated by comparing them with PBE-D3/def2-TZVPP calculations: similar results were obtained in all cases. All calculations were performed with the TURBOMOLE program package.

The calculations show that the S···S intramolecular interactions (indicated with dotted lines in Figure 1), favor the planar arrangement of adjacent rings (dihedral angle < 1 degree; S···S distance about 3.07–3.09 Å). Some torsional flexibility is observed instead in the bonds between bithiophene subsystems. As a result, a quaterthiophene made of two adjacent bithiophene subsystems is planar with a small distortion in the central bond (torsional angle of about 10 degrees) and a similar torsional angle is found for the central C–C bond of the octamer made of four bithiophene subsystems. This type of bonding pattern leads to the existence of two quasi-degenerate minimum-energy conformations for octamer **1**, separated by less than 1 kcal/mol in energy and differing for the relative orientation of the three main C–C torsional angles between bithiophene subsystems. The first slightly more stable conformation is characterized by torsions of opposite sign in the carbon-carbon single bonds and is therefore, on average, almost planar (**Figure 9**A). The second conformation, on the opposite, displays the three torsions in the same directions (Figure 9B) and is in consequence significantly twisted with respect to the main molecular axis. The orientation of the side chains was found to play a negligible role in gas phase, with the orientation perpendicular to the average molecular plane being slightly favored with respect to the orientation on the average molecular plane. When the aggregate formed by two stacked molecules is considered, the situation is different. In general, packing interactions shall favor the planarization of the octamer units, independently of whether the starting monomers were in the 'planar' or 'twisted' configuration. However, in this case, a significant role was found to be played by the orientation of the side chains. When the SCH_3 side groups lay in a planar configuration with respect to the octamer's main body, they do not contribute substantially to the intermolecular interaction. Therefore, the whole complex tends to be planar, due to the prevalence of stacking forces (Figure 9C). This geometrical configuration is ascribable to the yellow fibers. On the contrary, when a perpendicular configuration is considered for the side chains, steric interactions are present between the CH_3 units and the thiophene rings of the other molecule. As a result, small and diffuse distortions of the molecular backbone are promoted. In consequence, the complex assumes a twisted geometry (Figure 8D), which can be ascribed to the red fibers. We remark that, despite the conformational differences and the existence in the latter aggregate of steric interactions which promote a distortion of the molecular backbone, the binding interaction in both cases is determined by stacking forces. Therefore, since at room temperature the orientation of the side chains in non-aggregated octamer can be assumed to be random, we expect the two conformations to have very similar probabilities to form. Moreover, the presence of perpendicular side chains is only causing a small destabilization of the binding and the planar aggregate is only 27 kcal/mol lower in energy than the twisted one. Finally, to support our assignment of the two structures to the yellow and red microfibers, we performed additional time-dependent density functional theory calculations at the PBE/def2 -TZVPP level to compute the lowest optically active excited states of both systems. The calculations yielded a difference in excitation energy of 0.11 eV, compatible with the yellow-red color difference. Figure 9E,F shows a sketch comparing the proposed supramolecular organisation of the yellow and red microfibers. In both cases the molecules which, given the intense fluorescence signal, are likely to be in a J-type arrangement,[25] are organized in platelets forming crystalline domains. In the yellow microfibers the platelets are parallel with interchain stacking and strongly π–π interacting building blocks (Figure 9E). Instead, in the red microfibers, owing to the twisted conformation, the platelets tend to bend forming curves and curls (Figure 8F), as already described in reference[25]. The proposed model is in agreement with the difference in OFET charge mobility measured for the yellow and red microfibers. Indeed, in π-conjugated materials, charge transport takes place by interchain

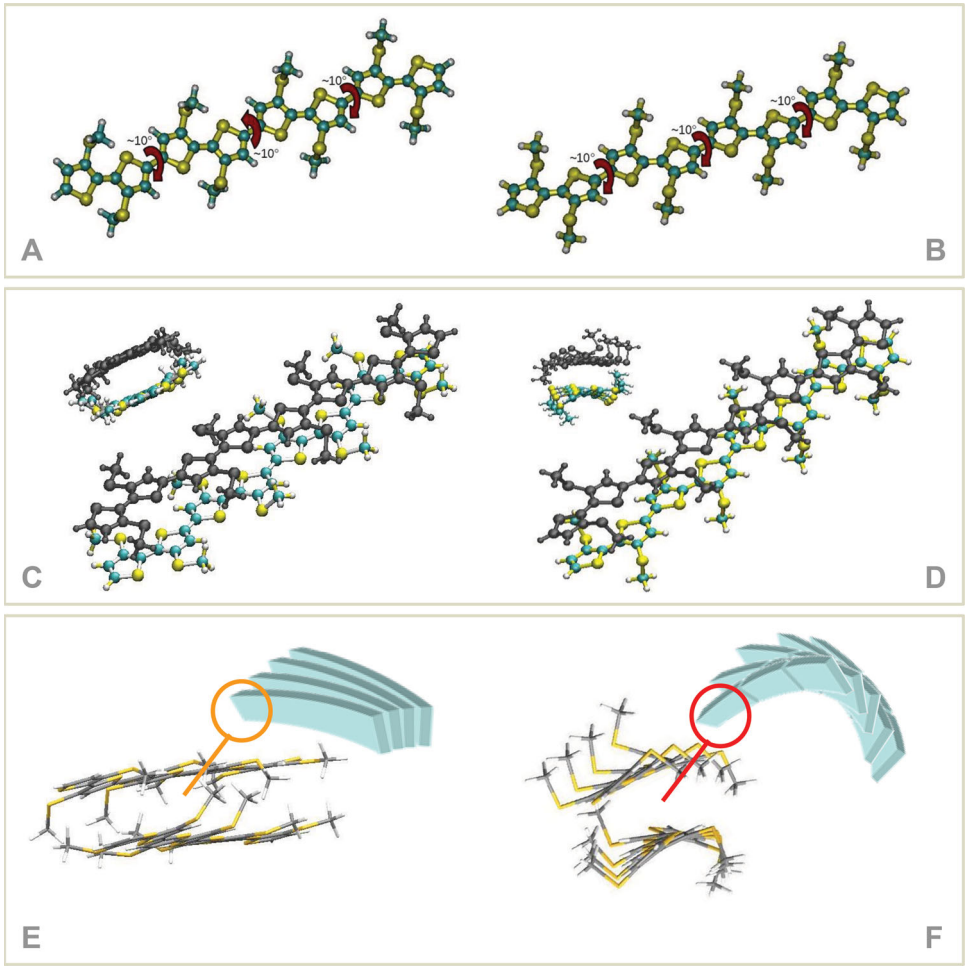

Figure 9. A,B) Calculated preferred conformations of octamer **5** (R = SCH_3). C,D) Calculatd geometries of the aggregate made of two molecules of **5** in **A** or **B** conformation. E,F) Sketch of the proposed supramolecular organization of the yellow and red microfibers.

hopping,[41] a mechanism which is is more efficient between parallel lamellae.

3. Conclusion

We reported the first case of fully characterized polymorphic, stable and crystalline, microfibers formed by an achiral octithiophene spontaneously self-assemblying at room temperature on several surfaces (glass, ITO, SiO_2/Au) with the same reproducible morphology. Theoretical evidence points to the microfibers as being the manifestation of *conformational* polymorphism. The control of the self-assembly process leads to polymorphic linear arrays of the octithiophene being micrometric in length and width and submicrometric in thickness, held together by non covalent interactions and displaying markedly different morphological and functional properties. The polymorphs, one made by straight and the other by helical microfibers, are not only fluorescent and electroactive but also chiral, with the latter being characterized by an additional supramolecular component of the CD spectrum. Incidentally, we note that the importance of addressing stereochemistry in the development and application of functional thiophene materials in the solid state has been largely overlooked so far. Our results indicate that in the field of thiophene oligomers and their supramolecular assemblies – very promising materials for application in photonics, biosensors, (opto)electronics – it is time to broadly use polymorph screening as a tool to control and optimise the quality and efficiency of the final materials, in analogy with what is currently done in pharmaceutical industry for drug substances.

Supporting Information

Supporting Information is available from the Wiley Online Library or from the author.

Acknowledgements

This work was supported by the *Laboratory of micro and submicro enabling technologies* (MIST E-R S.C.R.L.) of Emilia-Romagna, Italy.

Received: February 16, 2014
Revised: March 12, 2014
Published online: May 22, 2014

[1] J. P. Brog, C. L. Chanez, A. Crochet, K. M. Fromm, *RSC Adv.* **2013**, *3*, 16905–16931.
[2] R. J. Davey, S. L. M. Schroeder, J. H. ter Horst, *Angew. Chem. Int. Ed.* **2013**, *52*, 2166–2179.
[3] A. Nangia, *Acc. Chem. Res.* **2008**, *41*, 595–604.
[4] J. Chen, M. Shao, K. Xiao, Z. He, D. Li, B. S. Lokitz, D. K. Hensley, S. M. Kilbey, J. E. Anthony, J. K. Keum, A. J. Rondinone, W. Y. Lee, S. Hong, Z. Bao, *Chem. Mater.* **2013**, *25*, 4378–4386.
[5] J. Chen, M. Shao, K. Xiao, A. J. Rondinone, Y. L. Loo, P. R. C. Kent, B. G. Sumpter, D. Li, J. K. Keum, P. J. Diemer, J. E. Anthony, O. D. Jurchescu, J. Huang, *Nanoscale* **2014**, *6*, 449–456.
[6] S. Schiefer, M. Huth, A. Dobrinevski, B. Nickel, *J. Am. Chem. Soc.* **2007**, *129*, 10316–10317.
[7] X. Gu, J. Yao, G. Zhang, Y. Yan, C. Zhang, Q. Peng, Q. Liao, Y. Wu, Z. Xu, Y. Zhao, H. Fu, D. Zhang, *Adv. Funct. Mater.* **2012**, *22*, 4862–4872.
[8] A. G. Dikundwar, G. K. Dutta, T. N. Guru Row, S. Patil, *Cryst. Growth Des.* **2011**, *11*, 1615–1622.
[9] C. Poelking, D. Andrienko, *Macromol.* **2013**, *46*, 8941–8956.
[10] F. P. V. Koch, M. Heeney, P. Smith, *J. Am. Chem. Soc.* **2013**, *135*, 13699–13709.
[11] Y. Yuan, J. Zhang, J. Sun, J. Hu, T. Zhang, Y. Duan, *Macromol.* **2011**, *44*, 9341–9350.
[12] J. Bernstein, A. T. Hagler, *J. Am. Chem. Soc.* **1978**, *100*, 673–681.
[13] J. Bernstein, *Acc. Chem. Res.* **1995**, *28*, 193–200.
[14] L. Yu, *Acc. Chem. Res.* **2010**, *43*, 1257–1266.
[15] S. Chen, I. A. Guzei, L. Yu, *J. Am. Chem. Soc.* **2005**, *127*, 9881–9885.
[16] L. Antolini, G. Horowitz, F. Kouki, F. Garnier, *Adv. Mater.* **1998**, *10*, 382–385.
[17] T. Siegrist, C. Kloc, R. A. Laudise, H. E. Katz, R. C. Haddon, *Adv. Mater.* **1998**, *10*, 379–382.
[18] T. Siegrist, R. M. Fleming, R. C. Haddon, R. A. Laudise, A. J. Lovinger, H. E. Katz, P. Bridenbaugh, D. D. Davis, *J. Mater. Res.* **1995**, 2170–2173.
[19] F. Garnier, *Acc. Chem. Res.* **1999**, *32*, 209–215.
[20] G. Barbarella, M. Zambianchi, R. Di Toro, M. Colonna, L. Antolini, A. Bongini, *Adv. Mater.* **1996**, *8*, 327–330.
[21] G. Barbarella, M. Zambianchi, M. Del Fresno, I. Marimon, L. Antolini, A. Bongini, *Adv. Mater.* **1997**, *9*, 484–487.
[22] G. Barbarella, M. Zambianchi, L. Antolini, P. Ostoja, P. Maccagnani, A. Bongini, E. A. Marseglia, E. Tedesco, G. Gigli, G. R. Cingolani, *J. Am. Chem. Soc.* **1999**, *121*, 8920–8926.
[23] H. Pan, P. Liu, Y. Li, Y. Wu, B. S. Ong, S. Zhu, G. Xu, *Adv. Mater.* **2007**, *19*, 3240–3243.
[24] A. N. Sokolov, J. C. Sumrak, L. R. MacGillivray, *Chem. Commun.* **2010**, *46*, 82–84.
[25] F. Di Maria, P. Olivelli, M. Gazzano, A. Zanelli, M. Biasiucci, G. Gigli, D. Gentili, P. D'Angelo, M. Cavallini, G. Barbarella, *J. Am. Chem. Soc.* **2011**, *133*, 8654–8661.
[26] Ph. Leclère, M. Surin, P. Viville, R. Lazzaroni, A. F. M. Kilbinger, O. Henze, W. J. Feast, M. Cavallini, F. Biscarini, A. P. H. J. Schenning, E. W. Meijer, *Chem. Mater.* **2004**, *16*, 4452–4466.
[27] A. Brillante, I. Bilotti, F. Biscarini, R. G. Della Valle, E. Venuti, *E. Chem. Phys.* **2006**, *328*, 125–131.
[28] J. R. Lakowicz, *Principles of Fluorescence Spectroscopy*, 3rd Ed., Springer, Singapore **2006**.
[29] M. Sauer, J. Hofkens, J. Enderlein, *Handbook of Fluorescence Spectroscopy and Imaging*. Wiley-VCH Verlag GmbH & Co. KGaA, Weinheim **2011**.
[30] V. Vicinelli, G. Bergamini, P. Ceroni, V. Balzani, F. Vögtle, O. Lukin, *J. Phys. Chem. B* **2007**, *111*, 6620–6627.
[31] G. Bergamini, E. Marchi, P. Ceroni, V. Balzani, in *Designing Dendrimers* (Eds: S. Campagna, P. Ceroni, F. Puntoriero), John Wiley & Sons, Hoboken **2012**, Ch.*11*, pp. 341–366.
[32] J. Gierschner, M. Ehni, H. J. Egelhaaf, B. M. Medina, D. Beljonne, H. Benmansour, G. C. Bazan, *J. Chem. Phys.* **2005**, *123*, 144914.
[33] C. Simbrunner, *Semicond. Sci. Technol.* **2013**, *28*, 053001.
[34] E. L. Eliel, S. H. Wilen, L. N. Mander, *Stereochemistry of Organic Compounds*, John Wiley and Sons, New York **1994**, pp.1142–1145.
[35] J. Clayden, W. J. Moran, P. J. Edwards, S. R. LaPlante, *Angew. Chem. Int. Ed.* **2009**, *48*, 6398–6401.
[36] F. Leroux, *ChemBioChem* **2004**, *5*, 644–649.
[37] M. Suárez, N. Branda, J. M. Lehn, A. Decian, J. Fischer, *Helv. Chim. Acta* **1998**, *81*, 1–13.
[38] *Top. Curr. Chem. Supramolecular Chirality* (Eds: M. Crego-Calama, D. N. Reinhoud), Vol. *265*, Springer, Berlin **2006**.
[39] N. Micali, H. Engelkamp, P. G. van Rhee, P. C. M. Christianen, L. Monsù Scolaro, J. C. Maan, *Nat. Chem.* **2012**, *4*, 201–207.
[40] J. Xu, S. Semin, D. Niedzialek, P. H. J. Kouwer, E. Fron, E. Coutino, M. Savoini, Y. Li, J. Hofkens, H. Uji-I, D. Beljonne, T. Rasing, A. E. Rowan, *Adv. Mater.* **2013**, *25*, 2084–2089.
[41] C. Wang, H. Dong, W. Hu, Y. Liu, D. Zhu, *Chem. Rev.* **2012**, *112*, 2208–2267.
[42] D. Gentili, F. Di Maria, F. Liscio, L. Ferlauto, F. Leonardi, L. Maini, M. Gazzano, S. Milita, G. Barbarella, M. Cavallini, *J. Mater. Chem.* **2012**, *22*, 20852–20856.
[43] L. A. Constantin, E. Fabiano, F. Della Sala, *F. J. Chem. Theory Comput.* **2013**, *9*, 2256–2263.